Available online at www.sciencedirect.com
ScienceDirect
Journal of Sound and Vibration 319 (2009) 606–621
JOURNAL OF SOUND AND VIBRATION
www.elsevier.com/locate/jsvi

Numerical and analytical modelling of trapped gas in micromechanical squeeze-film dampers

Timo Veijola*, Anu Lehtovuori

Department of Radio Science and Engineering, Helsinki University of Technology, P.O. Box 3000, FIN-02015 TKK, Finland

Received 27 December 2007; received in revised form 20 May 2008; accepted 28 May 2008
Handling Editor: C.L. Morfey
Available online 24 July 2008

Abstract

Damping in air gaps of micromechanical devices that vibrate out-of-plane is studied at frequencies where the acoustic wavelength is comparable with the air gap dimensions. A FEM study with a viscoacoustic solver shows that above a certain frequency, closed damper borders can be assumed in the approximate analysis of the squeeze-film damper, regardless of the practical border conditions. Here, this closed-border (trapped gas) problem is solved analytically from the linearized Navier–Stokes equations in 1D. This results in a compact model for the mechanical impedance that accounts for damping, inertial and spring forces as well as thermal behaviour and slip border conditions. The model produces the gas resonances in the air gap when the wavelength of the acoustic wave is smaller than the gap dimensions. Due to the slip conditions, the model is valid in modeling micromechanical oscillating structures with small air gaps.
© 2008 Elsevier Ltd. All rights reserved.

1. Introduction

Damping in air gaps of out-of-plane oscillating structures has been traditionally modelled with the Reynolds equation [1,2]. It has been derived by simplifying the Navier–Stokes equations assuming a small air gap compared with the length or width of the damper surface, negligible inertial forces (Reynolds number $\ll 1$) and isothermal conditions. The Reynolds equation considers the viscous gas flow and compressibility in a thin air gap assuming constant pressure across the small gap and is usable only up to a certain frequency. The applicable frequency range can be extended considering also the inertia in the gap flow [3–6], together with the non-isothermal behaviour [7–9]. These models work in the region where the acoustic wavelength is comparable with the dimensions of the damper surface, but they still assume constant pressure across the air gap and an acoustic wavelength much larger than the air gap height.

At higher frequencies where the length of the acoustic wave is comparable to the height of the air gap, the pressure is no more constant across the air gap. Moreover, neither isothermal nor adiabatic assumptions can be made, and temperature variation and thermal conductivity must be accounted for in the model. This leads to another damping mechanism in addition to viscous damping.

*Corresponding author. Fax: +358 9 451 4818.
E-mail address: timo.veijola@tkk.fi (T. Veijola).

0022-460X/$ - see front matter © 2008 Elsevier Ltd. All rights reserved.
doi:10.1016/j.jsv.2008.05.038

When the small air gap separations of micromechanical devices are considered, the continuum boundary conditions no more apply. Several papers discuss the modified Reynolds equation that considers the change in the flow rate vs. the Knudsen number [10–13]. These models are valid at a large range of Knudsen numbers, but they assume a low Reynolds number. The model in Ref. [6] considers the gas inertia and the gas rarefaction in the slip flow regime (Knudsen number $K_n < 0.1$).

A FEM study with a viscoacoustic solver in this paper shows that above a certain frequency the wave propagation in the air gap takes place only in the out-of-plane direction (except for the region close to the borders), indicating a fully trapped gas situation. That is, in the analysis above a certain frequency, closed damper borders can be assumed regardless of any border conditions. This assumption simplifies the analysis considerable, since the topology of the damper becomes insignificant, and only the surface area needs to be considered.

Several papers study the behaviour of oscillating visco-thermal fluid in small air gaps with a varying pressure distribution across the gap [14–18]. These studies concentrate on the viscoacoustic problem of gas between a vibrating membrane and a backing wall, and wave propagation in two directions has been included in these models. Generally, open border conditions are assumed, but Bruneau et al. [15] have given a solution for finite specific impedance at the periphery. These studies concentrate on frequencies below the air gap resonances; they do not consider slip boundary conditions nor the viscous stress term in the force acting on the surface.

In this paper, the emphasis is on operation at frequencies above the classical acoustic frequencies where the gas can be assumed to be fully trapped in the gap. The linearized Navier–Stokes (N–S) equations are presented and reduced to a 1D model for the closed border (fully trapped gas) situation. The variables are the pressure, density, velocity and temperature that all vary across the gap. The equations are solved analytically taking into account the boundary conditions. Due to the small dimensions in micromechanical devices, slip conditions are used for temperature [19]. Velocity slip conditions are not needed here due to the trapped gas. In this paper, two different solutions are presented: a simple model that assumes adiabatic conditions, and an exact model that considers varying thermal conditions between isothermal and adiabatic.

2D FEM simulations with a viscoacoustic solver (linearized N–S equations) were used to verify the derived models. The behaviour of the damping and spring forces are demonstrated, and the responses of the exact and the simple models are compared.

2. Viscoelastic wave propagation model

In this chapter, a wave propagation model for a trapped gas situation is derived for the structure shown in Fig. 1. In practice, the upper plane represents a surface of a vibrating body, and there is no gas flow above this plane. The figure shows the dimensions of the damper surface (l_x, l_y) and the air gap h_0. Normalized coordinates (x, y and z) are used below instead of the absolute coordinates ($\overline{x}$, $\overline{y}$ and $\overline{x}$) shown in the figure. The same notation applies to the variables used. The upper surface moves and acts on the gas in the air gap between the surfaces.

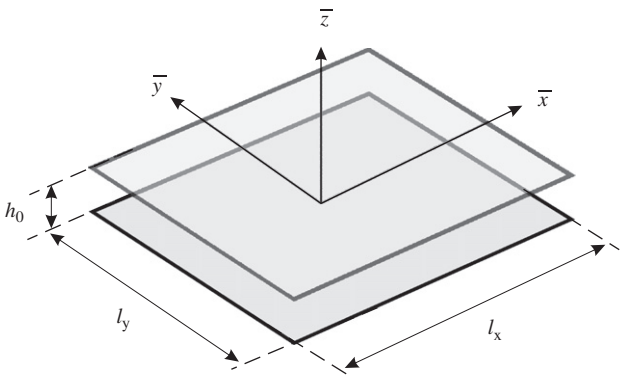

Fig. 1. A squeeze-film damper consisting of parallel surfaces moving perpendicularly.

2.1. Variables

A frequency-domain analysis with small perturbation amplitudes at the angular frequency ω is assumed. p, ρ and T represent small relative variations around static pressure p_0, density ρ_0 and temperature T_0, respectively. Equations are presented in normalized form. The small-amplitude perturbation variables are specified with

$$\overline{p} = p_0(1 + p\mathrm{e}^{\mathrm{i}\omega t}), \quad \overline{T} = T_0(1 + T\mathrm{e}^{\mathrm{i}\omega t}), \quad \overline{\rho} = \rho_0(1 + \rho\mathrm{e}^{\mathrm{i}\omega t}). \tag{1}$$

u, v and w are velocity components in the x-, y- and z-directions, respectively. The equations will be presented in normalized form such that velocities u, v and w are normalized to the adiabatic speed of sound c_0, while the dimensions x, y and z are normalized with the characteristic dimensions l_x, l_y and h_0, respectively.

2.2. Damping and spring forces

The damper is characterized here with a mechanical impedance Z_m, that is calculated from the force $\overline{F}$ acting on the moving upper surface having a velocity of $\overline{w}_0$ in the z direction:

$$Z_m = -\frac{\overline{F}}{\overline{w}_0} = -\frac{l_x l_y p_0 F}{c_0 w_0}. \tag{2}$$

The damping coefficient $c = \mathrm{Re}(Z_m)$ (real part of Z_m), and the spring constant is $b = -\omega\,\mathrm{Im}(Z_m)$, where $\mathrm{Im}(Z_m)$ is the imaginary part of Z_m.

2.3. Characteristic numbers

The behaviour of the flow in a narrow air gap is described in the frequency domain by a few characteristic numbers. The Reynolds number Re (the square of the shear wave number s) is the ratio between inertial and viscous forces:

$$s^2 = Re = \frac{\omega h_0^2 \rho_0}{\mu}, \tag{3}$$

where μ is the viscosity coefficient and h_0 is the characteristic height of the air gap.

The reduced frequency $k = \omega h_0/c_0$ is scaled with the nominal gap displacement h_0 and the adiabatic speed of sound $c_0 = \sqrt{\gamma p_0/\rho_0}$, where γ is the specific heat ratio.

The Knudsen number $K_n = \lambda/h_0$ is a measure of gas rarefaction and λ is the mean free path. The Prandtl number Pr characterizes the thermal properties. Here, the square root of Pr is used,

$$\phi = \sqrt{Pr} = \sqrt{\frac{\mu C_p}{\kappa}}, \tag{4}$$

where C_p is the specific heat at constant pressure and κ is the thermal conductivity.

K_T is the "thermal Knudsen number" [19] that characterizes the temperature jump at the surfaces due to rarefied gas

$$K_T = \frac{2 - \alpha_T}{\alpha_T}\left[\frac{2\gamma}{\gamma + 1}\right]\frac{K_n}{\phi^2}, \tag{5}$$

where α_T is the energy accommodation coefficient.

2.4. Linearized Navier–Stokes equations

The dimensionless notation by Beltman [8] is used here for the linearized time-harmonic Navier–Stokes equations:

$$\mathrm{i}u = -\frac{g}{k\gamma}\frac{\partial p}{\partial x} + \frac{1}{s^2}\left[g^2\frac{\partial^2 u}{\partial x^2} + \left(\frac{g}{a}\right)^2\frac{\partial^2 u}{\partial y^2} + \frac{\partial^2 u}{\partial z^2}\right] + \frac{1}{3}\frac{g}{s^2}\frac{\partial}{\partial x}\left[g\frac{\partial u}{\partial x} + \left(\frac{g}{a}\right)\frac{\partial v}{\partial y} + \frac{\partial w}{\partial z}\right], \tag{6}$$

$$\mathrm{i}v = -\frac{g}{ak\gamma}\frac{\partial p}{\partial y} + \frac{1}{s^2}\left[g^2\frac{\partial^2 v}{\partial x^2} + \left(\frac{g}{a}\right)^2\frac{\partial^2 v}{\partial y^2} + \frac{\partial^2 v}{\partial z^2}\right] + \frac{1}{3}\frac{g}{as^2}\frac{\partial}{\partial y}\left[g\frac{\partial u}{\partial x} + \left(\frac{g}{a}\right)\frac{\partial v}{\partial y} + \frac{\partial w}{\partial z}\right], \tag{7}$$

$$\mathrm{i}w = -\frac{1}{k\gamma}\frac{\partial p}{\partial z} + \frac{1}{s^2}\left[g^2\frac{\partial^2 w}{\partial x^2} + \left(\frac{g}{a}\right)^2\frac{\partial^2 w}{\partial y^2} + \frac{\partial^2 w}{\partial z^2}\right] + \frac{1}{3}\frac{1}{s^2}\frac{\partial}{\partial z}\left[g\frac{\partial u}{\partial x} + \left(\frac{g}{a}\right)\frac{\partial v}{\partial y} + \frac{\partial w}{\partial z}\right], \tag{8}$$

$$g\frac{\partial u}{\partial x} + \frac{g}{a}\frac{\partial v}{\partial y} + \frac{\partial w}{\partial z} = -\mathrm{i}k\rho, \tag{9}$$

$$p = \rho + T, \tag{10}$$

$$\mathrm{i}T = \frac{1}{s^2\phi^2}\left[g^2\frac{\partial^2 T}{\partial x^2} + \left(\frac{g}{a}\right)^2\frac{\partial^2 T}{\partial y^2} + \frac{\partial^2 T}{\partial z^2}\right] + \mathrm{i}\frac{\gamma-1}{\gamma}p. \tag{11}$$

The height of the gap $g = h_0/l_x$ and ratio of the plate $a = l_y/l_x$ are as shown in Fig. 1. The equations above assume zero bulk viscosity $\beta = \frac{2}{3}\mu + \eta$, where the second viscosity coefficient, η, is determined by the Stokes condition $\beta = 0$ [20,21].

3. 1D wave propagation model

In his "narrow gap" solution (Appendix B in Ref. [8]), Beltman simplifies Eqs. (6)–(11) assuming $g/s \ll 1$ and a negligible z-directional velocity w compared with the velocities u and v. Here the situation is different: a small gap is not assumed, but velocities u and v are assumed to be negligible due to the closed borders. This reflects the trapped gas situation. Now, the basic equations (6)–(11) degenerate to the following set of wave equations as an asymptote for increasing frequency:

$$\mathrm{i}w = -\frac{1}{k\gamma}\frac{\partial p}{\partial z} + \frac{4}{3s^2}\frac{\partial^2 w}{\partial z^2}, \tag{12}$$

$$\frac{\partial w}{\partial z} = -\mathrm{i}k\rho, \tag{13}$$

$$p = \rho + T, \tag{14}$$

$$\mathrm{i}T = \frac{1}{s^2\phi^2}\frac{\partial^2 T}{\partial z^2} + \mathrm{i}\frac{\gamma-1}{\gamma}p. \tag{15}$$

Instead of zero boundary conditions, slip boundary conditions for temperature T [19] are applied:

$$T|_{z=1} = -K_T\left.\frac{\partial T}{\partial z}\right|_{z=1}, \quad T|_{z=0} = K_T\left.\frac{\partial T}{\partial z}\right|_{z=0}. \tag{16}$$

The force F acting on the surface is due to the pressure and the viscous stress according to the Navier–Poisson law with zero bulk viscosity [21]

$$F = -p(1) + \left.\frac{4\gamma k}{3s^2}\frac{\partial w}{\partial z}\right|_{z=1}. \tag{17}$$

Since u and v were assumed to be negligible compared to w, only the spatial derivate in the z direction is needed in Eq. (17). Because of the relation Eq. (17), the force term for high frequencies depends on the viscosity μ.

3.1. Simple solution

First, a simplified case is studied to solve Eqs. (12)–(15). Since the model is derived here for relatively high frequencies, adiabatic thermal conditions are assumed. This simplifies Eq. (15) to

$$T = \frac{\gamma - 1}{\gamma} p \tag{18}$$

and the density from Eq. (14) results in $\rho = p/\gamma$. The isothermal assumption that is valid at low frequencies only would result in $\rho = p$. The pressure is solved from Eq. (13) resulting in

$$p = -\frac{\gamma}{\mathrm{i}k} \frac{\partial w}{\partial z}. \tag{19}$$

Eq. (12) describes the relation between pressure and velocity in the z-direction, and after inserting Eq. (19) into it, results in

$$\mathrm{i}w = \left(\frac{1}{\mathrm{i}k^2} + \frac{4}{3s^2}\right) \frac{\partial^2 w}{\partial z^2}. \tag{20}$$

The velocity function

$$w(z) = \frac{w_0 \sinh(qz)}{\sinh(q)}, \tag{21}$$

where

$$q = -\mathrm{i}\left(\frac{1}{k^2} + \mathrm{i}\frac{4}{3s^2}\right)^{-1/2} \tag{22}$$

is a solution of Eq. (20) and satisfies the boundary conditions $w(1) = w_0$ and $w(0) = 0$. At low frequencies, $q \to 0$ and $w(z)$ approaches a linear velocity profile $w_0 z$ corresponding to the approximation by Beltman.

Using Eq. (19) for pressure and Eq. (21) for velocity, the force acting on the moving surface Eq. (17) becomes

$$F = \left(\frac{1}{\mathrm{i}k} + \frac{4k}{3s^2}\right) \frac{\gamma q w_0}{\tanh(q)} = \frac{\mathrm{i}k\gamma w_0}{q \tanh(q)} \tag{23}$$

and Eq. (2) gives the unnormalized mechanical impedance.

The pressure term dominates the force at low frequencies when $k^2/s^2 \ll 1$, and the viscous stress dominates at high frequencies when $k^2/s^2 \gg 1$. According to Eq. (17), the derivative $\partial w/\partial z$ determines alone the frequency dependency at high frequencies, since k/s^2 is a constant. The asymptotic force at high frequencies can be derived from Eq. (23) assuming $\tanh(q) = 1$. This asymptotic force is

$$F_\infty = \sqrt{\frac{4\mathrm{i}\gamma\mu\omega}{3p_0}}. \tag{24}$$

In Ref. [22], the viscous stress term in Eq. (17) was not considered in the model, resulting in an incorrect force at very high frequencies. Also, the model in Ref. [22] showed a good agreement with FEM simulations, but the reason was that only the simulated pressure term was considered in the comparison.

3.2. Resonant frequencies

The expression for resonant frequencies can be approximated from Eq. (23) assuming a large s compared to k (small viscosity). This simplifies q to $-\mathrm{i}k$. Resonances occur when the denominator in Eq. (23) is zero or

infinity. This happens when $iq = N\pi/2$, where $N = 1, 2, 3, \ldots$. Odd values of N give antiresonances, while even values of N give resonances. Assuming adiabatic conditions, the approximate Nth resonant frequency is

$$f_N = \frac{N}{4h_0}\sqrt{\frac{\gamma p_0}{\rho_0}} = \frac{Nc_0}{4h_0}. \tag{25}$$

The first antiresonance f_1 is especially interesting, since if the device is operated close to this frequency, a very small damping due to gas can be achieved. For air at atmospheric pressure, $f_1 = 87.7\,\text{MHz}$ for an air gap of $1\,\mu\text{m}$.

3.3. Exact solution

The exact solution for Eqs. (12)–(15) is presented in the appendix. The boundary conditions for velocity are $w(0) = 0$ and $w(1) = w_0$, and the temperature has slip conditions at the surfaces. The solution gives velocity w, pressure p, temperature T and density ρ of the gas as function of z. The calculation of these variables requires the evaluation of numerous complex auxiliary variables. The force on the upper surface is calculated with Eq. (A.37) in the appendix, and Eq. (2) gives the unnormalized mechanical impedance.

The appendix of Ref. [22] reports the exact solution with zero temperature boundary conditions only.

The asymptotic behaviour of the exact model at high frequencies is the same as the behaviour of the simple model in Eq. (24) since at high frequencies adiabatic thermal conditions can be assumed.

4. Model verification

4.1. 2D FEM simulations

FEM simulations were performed with a solver for dissipative acoustic flow [23] included in Elmer [24] multiphysics FEM software. It solves the linearized N–S equations (6)–(11), with, velocity and temperature slip conditions.

Fig. 2 shows the topology of the simulated 1D squeeze-film damper. It is assumed that the third dimension l_y is much larger than l_x, which justifies the study of the 2D gas flow in the cross-section. The gas is bounded by two rigid parallel surfaces, and the upper surface is oscillating with a small amplitude of w_0 in the z direction.

In this study, parameters for air at standard atmosphere conditions are used, see Table 1. The air gap height is $h_0 = 1\,\mu\text{m}$ and the length is $l_x = 10\,\mu\text{m}$ ($l_y = 1\,\text{m}$). The upper surface oscillates in the z-direction with a constant velocity amplitude of $1\,\text{m/s}$ ($\overline{w}_0 = 1$).

At the damper borders boundary conditions $p(\pm 1/2) = 0$ and $u(\pm 1/2) = 0$ were used for open and closed borders, respectively. Slip boundary conditions for temperature were used and ideally thermal conducting surfaces were assumed. A mesh of 8000 rectangular elements was used, and the simulation was performed at 81 frequencies from 10 kHz to 1 GHz. The mesh was refined close to the borders. Tests with a higher number of elements (12,000) gave the same results within a relative amplitude and phase changes of 0.4 % and 0.3°, respectively. The gas parameters are shown in Table 1.

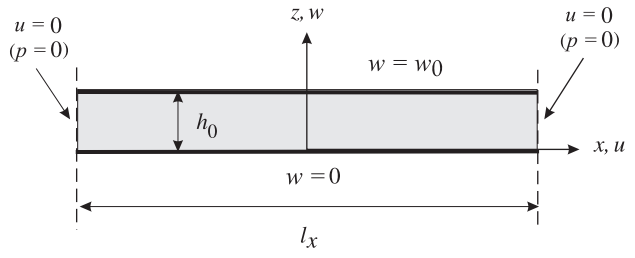

Fig. 2. The cross-section of squeeze-film damper. The y dimension of the damper l_y is assumed to be much larger than the x dimension l_x. Alternatively, closed borders ($u = 0$) or open borders ($p = 0$) are used.

Table 1
Gas parameters used in the simulations

	Description	Value	Unit
p_0	Pressure	100	$10^3\,\mathrm{N/m^2}$
T_0	Temperature	300	K
μ	Viscosity coefficient	18.5	$10^{-6}\,\mathrm{N\,s/m^2}$
ρ_0	Density of air	1.155	$\mathrm{kg/m^3}$
C_p	Specific heat	1.01	$10^3\,\mathrm{J/kg/K}$
γ	Specific heat ratio	1.4	
κ	Heat conductivity	0.025	W/m/K
λ	Mean free path	68.22	$10^{-9}\,\mathrm{m}$
α	Accommodation coefficient	1.0	
α_T	Thermal accommodation coefficient	1.0	

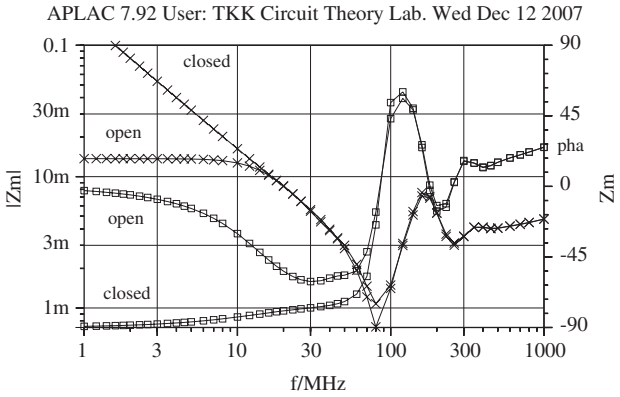

Fig. 3. Simulated amplitude (×) and phase (□) of Z_m for open and closed borders.

4.2. Open/closed damper boundaries

To demonstrate the trapping of the gas in the air gap at high frequencies, Fig. 3 shows forces acting on the upper surface as a function of frequency in two cases. First, the borders are assumed to be open (zero pressure); second, they are assumed to be closed (zero velocity). The amplitude responses are identical above a certain frequency indicating that at high frequencies, the flow velocity in the x direction becomes insignificant. The amplitude and phase responses are identical above 70 MHz ($k = 1.26$ and $s = 5.34$). This is close to the first resonant frequency at 88 MHz. Hence, at high frequencies the gas is trapped in the gap corresponding the closed border assumption, even for open border conditions.

Fig. 4 shows simulated pressure, velocity, and temperature amplitude distributions for the open border case at certain frequencies. These frequencies represent different flow regions that will be studied more closely. Frequency f_1 represents a small frequency, at which the pressure distribution across the gap is constant, and the velocity u out from the damper borders is considerable. f_1 and f_2 indicate the first and the second resonant frequencies. The maximum amplitudes for p, u, w and T in Fig. 4 are 200 Pa, 6.7 m/s, 1.8 m/s and 0.75 K, respectively.

The amplitude profiles in Fig. 4(b) show clearly that, at high frequencies f_1 and f_2, the velocity u in the x direction is independent of the x-coordinate, except very close to the borders. However, since the force has a minimum at f_1, any additional force component due to u might contribute considerably to the force at that frequency. Fig. 3 confirms this, since the relative deviation between the open border and closed border cases is maximum at $f_1 = 88$ MHz (except for the low-frequency regime). For a small gap to length ratio g, the

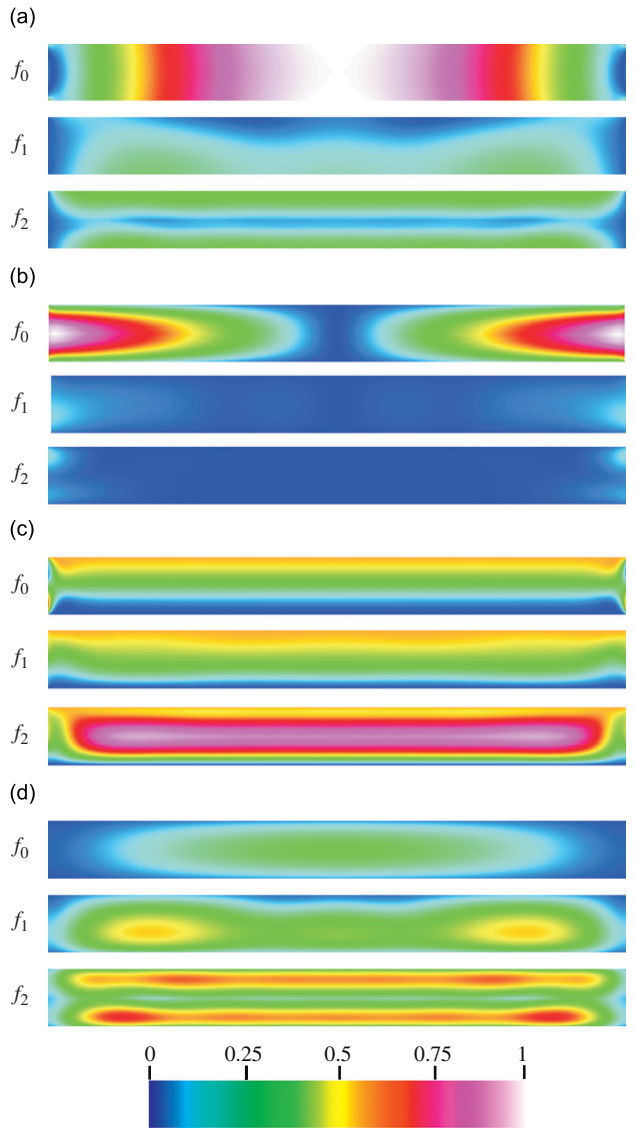

Fig. 4. Simulated relative amplitude profiles of (a) pressure $|p|$, (b) velocity $|u|$ in the x direction, (c) velocity $|w|$ in the z direction and (d) temperature $|T|$ at different frequencies in the case of open borders. Low-frequency regime $f_0 = 2.6\,\text{MHz}$ ($k = 0.047$ and $s = 1.0$), first resonance (force minimum) $f_1 = 80\,\text{MHz}$ ($k = 1.44$ and $s = 5.6$) and second resonance (force maximum) $f_2 = 180\,\text{MHz}$ ($k = 3.24$ and $s = 8.4$). Here $h_0 = 1\,\mu\text{m}$ and $l_x = 10\,\mu\text{m}$. (e) The colour scale used for relative amplitudes.

contribution of the borders is negligible, but for larger ratios, say 0.2, the closed-border assumption cannot be used in approximating the open-border situation at high frequencies.

Fig. 5 shows the pressure, velocity and temperature distributions in the air gap for the closed border case. These FEM simulations show clearly that the velocity in the x direction is zero and the other quantities do not depend on x.

4.3. Comparison between the simple and the exact model

Fig. 6 shows the difference between simple and exact solutions. The response of the exact model is identical with FEM simulation results made with closed borders. The resonant frequency of the simple solution matches well with the one calculated from Eq. (25). The difference between the amplitudes and phases are considerable, but the simple model does produce the same resonances as the exact model. The difference of the

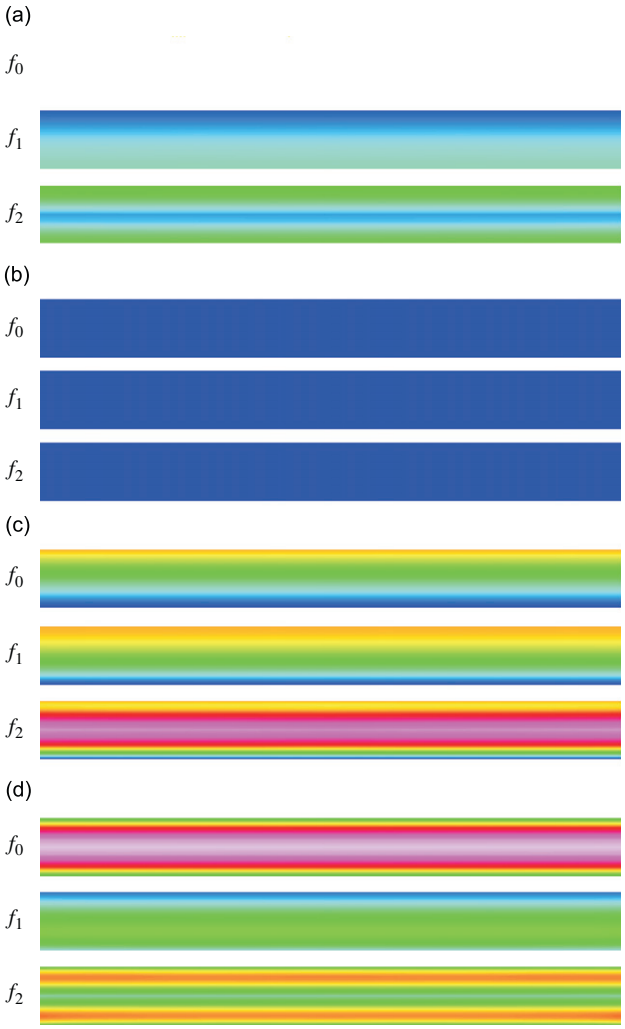

Fig. 5. Simulated relative amplitude profiles of (a) pressure $|p|$, (b) velocity $|u|$ in the x direction, (c) velocity $|w|$ in the z direction, and (d) temperature $|T|$ at different frequencies in the case of closed borders. Low-frequency regime $f_0 = 2.6\,\text{MHz}$ ($k = 0.047$ and $s = 1.0$), first resonance (force minimum) $f_1 = 80\,\text{MHz}$ ($k = 1.44$ and $s = 5.6$), and second resonance (force maximum) $f_2 = 180\,\text{MHz}$ ($k = 3.24$ and $s = 8.4$). Here $h_0 = 1\,\mu\text{m}$ and $l_x = 10\,\mu\text{m}$. The colour scale and the maximum amplitudes are the same as in Fig. 4.

two models is due to thermal behaviour. The simple model represents not only the adiabatic conditions, but also the case of a large Knudsen number K_n. This is not easy to see from the equations, but can be shown using the exact model.

Fig. 6 shows also the high-frequency asymptotic behaviour of the impedance calculated from Eq. (24). The contribution of the pressure term only in the force in Eq. (17) is also shown. The viscous stress term increases the force amplitude and inverts the phase at very high frequencies.

4.4. Damping coefficient and spring constant

When characterizing the fluid–structure interaction in practice, the damping coefficient and the spring constant are used: the damping coefficient determines the quality factor of the device and the spring coefficient determines the change in the mechanical resonant frequency. Fig. 7 presents the damping coefficient and the spring constant given by the model. Responses for two different air gap heights (a) $h_0 = 1\,\mu\text{m}$ and (b) $h_0 = 2\,\mu\text{m}$ are compared ($l_x = 10\,\mu\text{m}$). The damping coefficient $c = \text{Re}(Z_m)$ has a minimum at the first

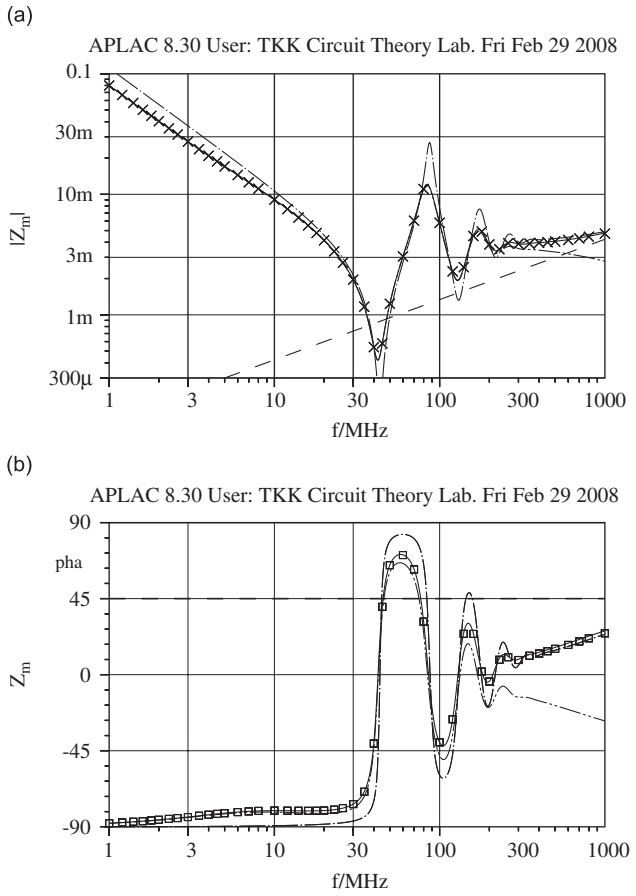

Fig. 6. Impedance Z_m (a) amplitudes and (b) phases calculated with the exact solution (——) compared with simple solution (— · — · —) and results of FEM simulation with closed borders (amplitudes × and phases □). The asymptotic impedance from Eq. (24) (— — —) and the exact model ignoring the viscous force term (— ·· — ·· —) are also shown in the figures.

resonance. When this minimum is matched with the resonance of the mechanical structure, the quality factor can be maximized.

The spring constant b is constant at small frequencies but goes below zero at the first resonance. A negative spring constant indicates inertial force, not a spring force. The inertial force dominates at very high frequencies.

4.5. *Profiles of variables*

Profiles of pressure p, temperature T and displacement w amplitudes at different frequencies are presented in Fig. 8. The exact model is used to compute the profiles. The pressure profile in Fig. 8(a) shows that at the first resonance frequency f_1, the pressure is small at $z = 1$ and at the second resonance frequency f_2 it is considerably larger. The velocity w in Fig. 8(b) satisfies the boundary conditions ($w(0) = 0$ and $w(1) = 1$), and shows an almost linear low-frequency response at f_0. At larger frequencies, the deviation from this linear behaviour is considerable. The temperature in Fig. 8(c) is not zero at the borders ($z = 0$ or $z = 1$), indicating a temperature jump due to rarefied gas.

5. Conclusions

FEM simulations show that both simple and exact models can be used in approximating the damping and spring forces due to gas accurately at frequencies that are larger than the first gap resonant frequency.

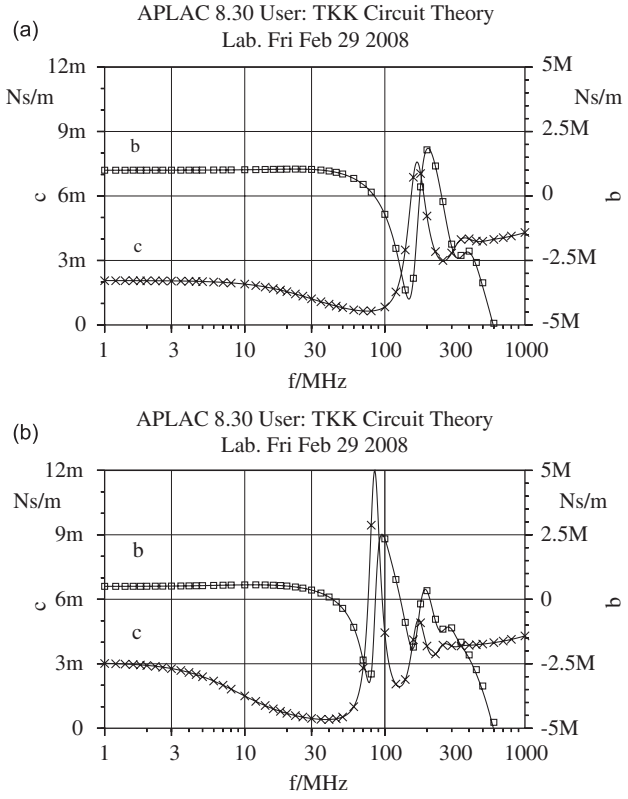

Fig. 7. Damping coefficient c in N s/m and the spring constant b in N/m as a function of frequency according to the exact model, and results of FEM simulation with closed borders (damping coefficient $\times$ and spring constant $\square$). (a) $h_0 = 1\,\mu\text{m}$ and (b) $h_0 = 2\,\mu\text{m}$.

This justified the derivation of the model for the closed border case. The accuracy of this approximation depends on the gap height to the surface dimension ratio. The results in Fig. 3 show that a ratio of 0.1, or smaller, is sufficient to keep the border effects small. The assumption of a 2D damper topology where l_y was much larger than l_x was made in the FEM simulations. This did not limit the applicability of the model to such structures, since the force does not depend on the shape of the surfaces in case of trapped gas.

Slip conditions were used to have an accurate model also for small air gaps in the slip flow regime $K_n < 0.1$. Neither the model nor the slip conditions are accurate outside the slip flow regime. However, the exact model shows that the model approaches the simple model for infinite K_n. Assuming that the same asymptotic behaviour as for the slip flow holds for the rarefied gas flow, the exact model gives a good approximation for any K_n.

The model shows that if the resonator can be designed such that the minimum of the damping coefficient matches the resonance of the device, then the quality factor can be maximized.

The comparison between the simple and exact models shows that for an accurate model, it is necessary to include the full temperature dependency in the model. However, the simple model gives a good estimate of the behaviour of the damping and spring forces.

The bulk viscosity was not considered here. Further studies would be required to study its influence.

The model can be applied in calculating the gas damping in air gaps of RF MEMS capacitively coupled resonators, such as a disk resonator [25–29]. Usage in modelling MEMS devices has been emphasized here, but the model is applicable also for larger gap heights and lower resonant frequencies, cases where slip conditions are not necessarily needed.

To have a compact model for a large frequency range from the viscous flow regime up to the frequencies where gap resonances occur, the presented model can be used as a building block.

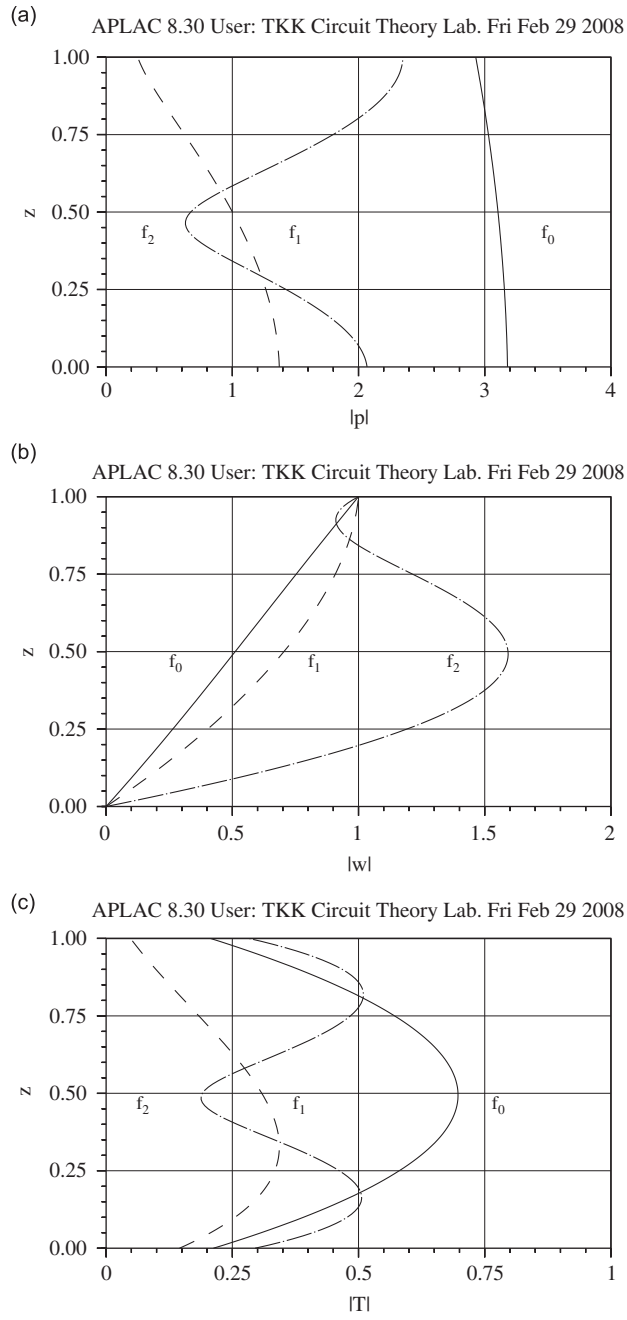

Fig. 8. Profiles of (a) pressure $|p|$, (b) velocity $|w|$ and (c) temperature $|T|$ at a few frequencies. $f_0 = 20\,\text{MHz}$ ($k = 0.36$ and $s = 2.8$) (——), $f_1 = 80.0\,\text{MHz}$ ($k = 1.44$ and $s = 5.6$) (– – –) is close to the first resonant frequency and $f_2 = 180\,\text{MHz}$ ($k = 3.24$ and $s = 8.4$) (— · — · —) is close to the second resonant frequency. The exact model is used here.

Appendix A. Exact solution

An exact solution for Eqs. (12)–(15) is presented considering the non-adiabatic thermal conditions and boundary conditions for velocity and temperature. After some manipulation, the following fourth-order

differential equation results:

$$\frac{1}{s^2\phi^2}\left(\frac{1}{\mathrm{i}k}+\frac{4k\gamma}{3s^2}\right)w''''-\left(\frac{\mathrm{i}4k}{3s^2}+\frac{\mathrm{i}k\gamma}{s^2\phi^2}+\frac{1}{k}\right)w''-kw=0 \tag{A.1}$$

for velocity w and

$$\frac{1}{s^2\phi^2}\left(\frac{1}{\mathrm{i}k}+\frac{4k\gamma}{3s^2}\right)T''''-\left(\frac{\mathrm{i}4k}{3s^2}+\frac{\mathrm{i}k\gamma}{s^2\phi^2}+\frac{1}{k}\right)T''-kT=0 \tag{A.2}$$

for temperature T as well. In this appendix, the derivatives with the respect to z are denoted with primes ($T''''=\partial^4T/\partial z^4$), and the dependence on z is denoted by, e.g., $w(z)$ or $T''''(z)$.

These homogenous linear equations with constant complex coefficients have a characteristic equation

$$\alpha_1r^4+\alpha_2r^2-k=0, \tag{A.3}$$

where

$$\alpha_1=\frac{1}{s^2\phi^2}\left(\frac{1}{\mathrm{i}k}+\frac{4k\gamma}{3s^2}\right), \tag{A.4}$$

$$\alpha_2=-\left(\frac{\mathrm{i}4k}{3s^2}+\frac{\mathrm{i}k\gamma}{s^2\phi^2}+\frac{1}{k}\right). \tag{A.5}$$

The roots of Eq. (A.3) are:

$$r_1=\sqrt{\frac{-\alpha_2+\sqrt{\alpha_2^2+4\alpha_1k}}{2\alpha_1}},\quad r_3=-r_1, \tag{A.6}$$

$$r_2=\sqrt{\frac{-\alpha_2-\sqrt{\alpha_2^2+4\alpha_1k}}{2\alpha_1}},\quad r_4=-r_2, \tag{A.7}$$

and thus the solution of Eq. (A.1) is

$$w(z)=C_1\mathrm{e}^{r_1z}+C_2\mathrm{e}^{r_2z}+C_3\mathrm{e}^{r_3z}+C_4\mathrm{e}^{r_4z}. \tag{A.8}$$

Constants C_1, C_2, C_3 and C_4 are determined using boundary conditions:

$$w(0)=0, \tag{A.9}$$

$$w(1)=w_0, \tag{A.10}$$

$$T(0)=K_TT'(0), \tag{A.11}$$

$$T(1)=-K_TT'(1). \tag{A.12}$$

Therefore, the temperature is written as function of velocity w. Eqs. (12)–(15) reduce now to

$$T'=A_1w+A_2w'', \tag{A.13}$$

$$w'=A_3T+A_4T'', \tag{A.14}$$

where

$$A_1=-\mathrm{i}k\gamma, \tag{A.15}$$

$$A_2=\left(\frac{1}{\mathrm{i}k}+\frac{4k\gamma}{3s^2}\right), \tag{A.16}$$

$$A_3 = -\frac{\mathrm{i}k}{\gamma - 1}, \tag{A.17}$$

$$A_4 = \frac{k\gamma}{(\gamma - 1)s^2\phi^2}. \tag{A.18}$$

Solving T from Eqs. (A.13) and (A.14) and p from Eqs. (13), (14) and (A.19) yields

$$T = B_1 w' + B_2 w''', \tag{A.19}$$

$$p = -\frac{1}{\mathrm{i}k} w' + T = \left(B_1 - \frac{1}{\mathrm{i}k}\right) w' + B_2 w''', \tag{A.20}$$

where B_1 and B_2 are the auxiliary variables:

$$B_1 = \frac{1 - A_1 A_4}{A_3}, \quad B_2 = -\frac{A_2 A_4}{A_3}. \tag{A.21}$$

Eq. (A.19) can be used to utilize the boundary conditions for temperature in Eqs. (A.11) and (A.12) to solve the velocity:

$$B_1 w'(0) + B_2 w'''(0) = K_T B_1 w''(0) + K_T B_2 w''''(0),$$

$$B_1 w'(1) + B_2 w'''(1) = -K_T B_1 w''(1) - K_T B_2 w''''(1).$$

After applying boundary conditions for velocity in Eqs. (A.9) and (A.10) in addition to the conditions above, the following system of equations results:

$$C_1 + C_2 + C_3 + C_4 = 0, \tag{A.22}$$

$$C_1 \mathrm{e}^{r_1} + C_2 \mathrm{e}^{r_2} + C_3 \mathrm{e}^{r_3} + C_4 \mathrm{e}^{r_4} = w_0, \tag{A.23}$$

$$C_1 Q_1 + C_2 Q_2 + C_3 Q_3 + C_4 Q_4 = 0, \tag{A.24}$$

$$C_1 S_1 \mathrm{e}^{r_1} + C_2 S_2 \mathrm{e}^{r_2} + C_3 S_3 \mathrm{e}^{r_3} + C_4 S_4 \mathrm{e}^{r_4} = 0, \tag{A.25}$$

where $Q_i = (B_1 r_i + B_2 r_i^3)(1 - K_T r_i)$ and $S_i = (B_1 r_i + B_2 r_i^3)(1 + K_T r_i)$. Solving the system of equations (A.22)–(A.25) gives the coefficients C_i in Eq. (A.8) which are:

$$C_1 = \frac{H_2 P_3 M - G P_3 - M P_2}{P_1 + P_2 L - H_1 P_3 - H_2 P_3 L}, \tag{A.26}$$

$$C_2 = L C_1 + M, \tag{A.27}$$

$$C_3 = G - H_1 C_1 - H_2 C_2, \tag{A.28}$$

$$C_4 = -C_1 - C_2 - C_3, \tag{A.29}$$

where

$$G = w_0/(\mathrm{e}^{r_3} - \mathrm{e}^{r_4}), \tag{A.30}$$

$$H_1 = (\mathrm{e}^{r_1} - \mathrm{e}^{r_4})/(\mathrm{e}^{r_3} - \mathrm{e}^{r_4}), \tag{A.31}$$

$$H_2 = (\mathrm{e}^{r_2} - \mathrm{e}^{r_4})/(\mathrm{e}^{r_3} - \mathrm{e}^{r_4}), \tag{A.32}$$

$$L = \frac{H_1 K_3 - K_1}{K_2 - H_2 K_3}, \tag{A.33}$$

$$M = \frac{-G K_3}{K_2 - H_2 K_3}, \tag{A.34}$$

$$K_i = B_1(r_i - r_4) + B_2(r_i^3 - r_4^3) - K_T B_1(r_i^2 - r_4^2) - K_T B_2(r_i^4 - r_4^4), \tag{A.35}$$

$$P_i = B_1(r_i e^{r_i} - r_4 e^{r_4}) + B_2(r_i^3 e^{r_i} - r_4^3 e^{r_4}) + K_T B_1(r_i^2 e^{r_i} - r_4^2 e^{r_4}) + K_T B_2(r_i^4 e^{r_i} - r_4^4 e^{r_4}). \tag{A.36}$$

Now the values for variables $p(z)$, $w(z)$, $T(z)$ can be calculated from Eqs. (A.20), (A.8) and (A.19), respectively. The density is simply $\rho(z) = p(z) - T(z)$.

The force on the upper surface is calculated with Eq. (17), resulting in

$$F = \left(\frac{1}{ik} + \frac{4\gamma k}{3s^2} - B_1\right) w'(1) - B_2 w'''(1), \tag{A.37}$$

where

$$w'(1) = C_1 r_1 e^{r_1} + C_2 r_2 e^{r_2} + C_3 r_3 e^{r_3} + C_4 r_4 e^{r_4}, \tag{A.38}$$

$$w'''(1) = C_1 r_1^3 e^{r_1} + C_2 r_2^3 e^{r_2} + C_3 r_3^3 e^{r_3} + C_4 r_4^3 e^{r_4}. \tag{A.39}$$

References

[1] J.J. Blech, On isothermal squeeze films, *Journal of Lubrication Technology* 105 (1983) 615–620.

[2] W.S. Griffin, H.H. Richardson, S. Yamanami, A study of fluid squeeze-film damping, *Journal of Basic Engineering, Transactions of the ASME* 88 (1966) 451–456.

[3] H.G. Elrod, Thin-film lubrication theory for newtonian fluids with surfaces possessing striated roughness or grooving, *Journal of Lubrication Technology* 94 (4) (1973) 484–489.

[4] S.R. Turns, Annular squeeze films with inertial effects, *Journal of Lubrication Technology* 105 (1983) 361–363.

[5] H. Hashimoto, Viscoelastic squeeze film characteristics with inertia effects between two parallel circular plates under sinusoidal motion, *Journal of Tribology, Transactions of the ASME* 116 (1994) 161–166.

[6] T. Veijola, Compact models for squeezed-film dampers with inertial and rarefied gas effects, *Journal of Micromechanics and Microengineering* 14 (2004) 1109–1118.

[7] M.J.H. Fox, P.N. Whitton, The damping of structural vibration by thin gas films, *Journal of Sound and Vibration* 73 (1980) 279–295.

[8] W.M. Beltman, P.J. van der Hoogt, R.M.E.J. Spiering, H. Tijdeman, Air loads on a rigid plate oscillating normal to fixed surface, *Journal of Sound and Vibration* 206 (1997) 217–241.

[9] W.M. Beltman, Viscothermal wave propagation including acousto-elastic interaction, part I: theory, *Journal of Sound and Vibration* 227 (1999) 555–586.

[10] S. Fukui, R. Kaneko, Analysis of ultra-thin gas film lubrication based on linearized Boltzmann equation: first report—derivation of a generalized lubrication equation including thermal creep flow, *Journal of Tribology, Transactions of the ASME* 110 (1988) 253–262.

[11] S. Fukui, R. Kaneko, A database for interpolation of Poiseuille flow rates for high Knudsen number lubrication problems, *Journal of Tribology, Transactions of the ASME* 112 (1990) 78–83.

[12] T. Veijola, H. Kuisma, J. Lahdenperä, T. Ryhänen, Equivalent circuit model of the squeezed gas film in a silicon accelerometer, *Sensors and Actuators A* 48 (1995) 239–248.

[13] P. Bahukudumbi, A. Beskok, A phenomenological lubrication mode for the entire Knudsen regime, *Journal of Micromechanics and Microengineering* 13 (2003) 873–884.

[14] G. Plantier, M. Bruneau, Heat conduction effects on the acoustic response of a membrane separated by a very thin air film from a backing electrode, *Journal Acoustique* 3 (1990) 243–250.

[15] M. Bruneau, A.M. Bruneau, P. Hamrey, An improved approach to modeling the behaviour of thin fluid films trapped between a vibrating membrane and a backing wall and surrounded by a reservoir at the periphery, *Acta Acustica* 1 (1993) 227–234.

[16] W.M. Beltman, Viscothermal wave propagation including acousto-elastic interaction, part II: applications, *Journal of Sound and Vibration* 227 (1999) 587–609.

[17] W.M. Beltman, Viscothermal wave propagation including acousto-elastic interaction, *Journal of the Acoustical Society of America* 116 (2004) 2542.

[18] C. Karra, M. Ben Tahar, Effects of entropic wave in vibroacoustic problem using boundary element analysis, *Flow, Turbulence and Combustion* 74 (2005) 49–66.

[19] G.E. Karniadakis, A. Beskok, *Micro Flows, Fundamentals and Simulation*, Springer, Heidelberg, 2002.

[20] R.E. Graves, B.M. Argrow, Bulk viscosity: past to present, *Journal of Thermophysics and Heat Transfer* 13 (1999) 337–342.

[21] L.E. Malvern, *Introduction to the Mechanics of a Continuous Medium*, Prentice-Hall, Inc., Prentice, 1969.

[22] T. Veijola, A. Lehtovuori, Model for gas damping in air gaps of RF MEMS resonators, in: *Symposium on Design, Test, Integration and Packaging of MEMS/MOEMS, DTIP 2007*, Stresa, Italy, 2007, pp. 156–161.

[23] M. Malinen, M. Lyly, P. Råback, A. Kärkkäinen, L. Kärkkäinen, A finite element method for the modeling of thermo-viscous effects in acoustics, in: P. Neittaanmäki, T. Rossi, K. Majava, O. Pironneau (Eds.), *Proceedings of the Fourth European Congress on Computational Methods in Applied Sciences and Engineering*, Jyväskylä, Finland, 2004.

[24] Elmer, Elmer—finite element solver for multiphysical problems, http://www.csc.fi/elmer, 2006.
[25] B. Bircumshaw, et al., The radial bulk annular resonator: towards a 50 Ω RF MEMS filter, *Proceedings of Transducers'03*, Boston, MA, 2003, pp. 875–878.
[26] J.R. Clark, W.-T. Hsu, C.T.-C. Nguyen, High-Q VHF micromechanical contour-mode disk resonators, *Technical Digest IEEE International Electron Devices Meeting*, 2000, pp. 493–496.
[27] J.W. Wang, Z. Ren, C.T.-C. Nguyen, 1156-GHz self-aligned vibrating micromechanical disk resonator, *IEEE Transactions on Ultrasonics, Ferroelectrics, and Frequency Control* 51 (12) (2004) 1607–1628.
[28] Z. Hao, S. Pourkamali, F. Ayazi, VHF single-crystal silicon elliptic bulk-mode capacitive disk resonators—part I: design and modeling, *Journal of Microelectromechanical Systems* 13 (2004) 1043–1053.
[29] S. Pourkamali, Z. Hao, F. Ayazi, VHF single-crystal silicon elliptic bulk-mode capacitive disk resonators—part I: implementation and characterization, *Journal of Microelectromechanical Systems* 13 (2004) 1054–1062.